CHALMERS
UNIVERSITY OF TECHNOLOGY

LOW-SPEED PROPELLER FOR UAV APPLICATIONS, FROM DESIGN TO EXPERIMENTAL EVALUATION

LOW-SPEED PROPELLER FOR UAV APPLICATIONS, FROM DESIGN TO EXPERIMENTAL EVALUATION

Michael Crona[1], Simon Dinger[1], Per Samuelsson[1], Hjalmar Strömfeldt[1] & Isak Jonsson[1]

[1]Chalmers University of Technology, Gothenburg, SE-41296, Sweden

Abstract

This paper presents the design and evaluation of a low-speed UAV propeller using OPTOPROP, a blade element momentum theory (BEMT) design tool. The integration of XFOIL allows for the generation and analysis of new propeller airfoils, such as NACA 4-digit series, optimized for low Reynolds number operation. This integration improves the estimated efficiency match between BEMT and CFD predictions by up to 10 percentage points. The study includes CFD analysis and wind tunnel tests, demonstrating the enhanced performance and efficiency of custom-designed propellers for low-speed UAV applications.

Keywords: BEMT, Propeller, CFD, Experimental

1. Introduction

Developing a propeller for low-speed, low-altitude cruise conditions is essential to optimize UAV performance. Commercial propellers available in this category are typically fixed-pitch and not designed to meet specific requirements, forcing designers to choose from a limited range of sizes and performance characteristics. Consequently, there are instances where no suitable propeller is available on the market. Previous research at Chalmers has shown that for small UAVs, this mismatch can cause efficiency losses of up to 20%, compelling designers to either adjust mission parameters or develop custom propellers. This work addresses this challenge by presenting the design and implementation of a tailored propeller optimized for these specific conditions. This work was done as part of a course at Chalmers University of Technology, Sweden.

1.1 Propeller Performance

Propeller performance [1] are typically represented with a group of nondimensional parameters such as thrust coefficient, C_T, power coefficient C_P, advance ratio J, and propeller efficiency (η_p) which are all defined in Eq. (1).

$$C_T = \frac{T}{\rho n^2 D^4} \qquad C_P = \frac{P}{\rho n^3 D^5} \qquad J = \frac{V_\infty}{nD} \qquad \eta_p = \frac{TV_\infty}{P} = \frac{C_T}{C_P} J \tag{1}$$

The ideal propulsive efficiency (η_p^*) using actuator disk theory, represents the inviscid losses related to the propwash acceleration. Its definition is presented in Eq. (2) and is used throughout this work as a benchmark.

$$\eta_p^* = \frac{2}{1 - v_s/V_\infty} \tag{2}$$

1.2 Blade Element Momentum Theory

Blade Element Momentum theory (BEMT) models are commonly applied for propeller design and analysis. The basis of the theory is that each section, or blade element, along the radius is considered as a separate (noninteracting) airfoil, represented by an airfoil geometry with associated coefficients of drag and lift for the specified operational condition. Aerodynamic forces are calculated for each element and integrated over the span of the rotating propeller to assess the overall performance. OPTOPROP is an in-house propeller design tool used at Chalmers University of Technology. The tool use BEMT design algorithms to generate propeller geometries and to estimate performance. OTPOPROP was benchmarked for the NACA 16-series in [6].

1.3 Reynolds Effects on Airfoil Performance

In the low-speed regime, the lift-to-drag ratio of an airfoil typically increases with the Reynolds number as shown in [3]. In OPTOPROP, the airfoil data used is derived from the NACA 16-series of airfoils, with properties experimentally established for Reynolds values not extending below 700,000 [8, 4]. The operating Reynolds number for the UAV propeller is estimated to reach a maximum of approximately 100,000. This discrepancy may cause OPTOPROP to overestimate propeller efficiency for operations at low Reynolds numbers.

2. Approach

To evaluate the performance of the design tool, a representative mission is selected, based on previously established requirements [5], where a drone with a mass of 8 kg and a lift-to-drag ratio of 20 is cruising at 25 m/s. Propellers are generated using OPTOPROP and subsequently evaluated using CFD. Propellers are then 3D printed and tested in the Chalmers low-turbulence wind tunnel. The focus of the present work is on the discrepancies found in the thrust and efficiency predictions of OPTOPROP and the validated CFD results. If those differences are well understood and established, the design parameters can be tuned in order to generate a propeller matching the required installed performance. In total, three propeller geometries are generated. V_1 is generated using the NACA 16-series airfoil, and V_2 using identical design parameters but with the NACA 4-series airfoil using data valid at lower Reynolds numbers. Another geometry, V_3 is generated using inputs similar to V_2, with an increased required thrust. This is done to match thrust deficiencies found in CFD analysis of the V_2 design.

3. Propeller Design

To optimize efficiency, two-bladed propellers were designed using the BEMT tool OPTOPROP. The inputs provided consists of a thrust requirement, a chord length distribution, blade count, and operational velocity. Several diameters and rotational speeds are subsequently evaluated given these inputs using OPTOPROP. The result allows for the selection of a suitable diameter and angular velocity as a trade-off between efficiency and propeller size.

In order to implement airfoil data suitable at low Reynolds numbers, XFOIL was used to estimate performance data for the NACA 4-digit series of airfoils at representative Reynolds numbers. Due to XFOIL instabilities, a Python wrapper was utilized to extract and store lift and drag coefficients for different airfoils. In cases where XFOIL failed to generate an airfoil, interpolation of performance data was used. The stored values could be called directly by OPTOPROP, removing the need to run XFOIL repeatedly. Airfoil geometries were generated using formulas derived from [2].

4. Numerical Setup

The propellers were numerically evaluated in Star-CCM+ using the Reynolds Averaged Navier-Stokes (URANS) equations with $k-\omega$ turbulence model. The rotating frame model was used to simulate the propeller motion. The domain was meshed using the Star-CCM+ grid generator, and it is comprised by prism layers near the propeller surfaces to adequately resolve the boundary layer, a high-resolution polyhedral domain is generated for the bulk rotating frame, assuming a 1.1 growth rate and relatively sparse tetrahedral cells in the outer domain. The average y^+ at the 75% propeller radius is less than one. Figure 1(a) shows the numerical domain, where the rotational part is marked in yellow. In contrast to a standard mesh, a rotational mesh adapts dynamically to the propeller's rotation,

allowing for a more accurate interaction between the fluid and the propeller. A mesh sensitivity study was conducted, for which the results are shown in Fig. 1(b) with respect to the relative variation in propeller efficiency. A mesh of $6.2 \cdot 10^6$ elements was selected to provide satisfactory results with rapidly diminishing returns with further refinement.

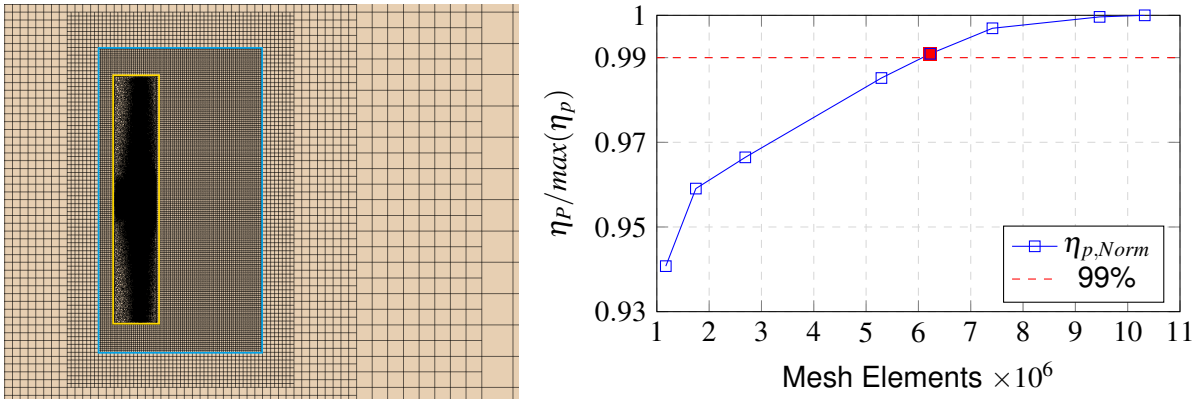

(a) (b)

Figure 1 – Side view of the numerical domain (a) and the mesh independent study (b) showing different evaluated resolutions as blue solid line and selected resolution as red solid marker.

5. Experimental Setup

The propellers were tested in the Chalmers low turbulence wind tunnel with a test chamber measuring 1.25m $\times$ 1.8m $\times$ 3m. More details of the tunnel can be found in [7]. An in-house manufactured propeller test bench was used. A schematic of the test bench is illustrated in Fig. 2. A 15V AC-DC converter powers a HobbyWing Platinum Pro 25A V4 ESC, which controls an EMAX GT3520 brushless outrunner motor that provides power to the propeller. The propeller is mounted on the outrunner part of the motor (shown as blue in Fig.2) using four M3 screws. The thrust of the propeller is measured via a DYLY-106 3kg load cell tension sensor (shown as red in Fig.2) mounted in line with the motor and propeller shaft. The torque is measured using two 1kg load cells (shown as red in Fig.2) mounted in parallel with the horizontal plane of the rotational axis, spaced 45mm apart and centered around the rotational axis. The torque is deduced from the sum of the load cells' outputs multiplied by the tangential vector around the rotational axis.

The load cell data is collected using a National Instruments cRio NI-9237 module at 25 kS/s/channel, configured for a full-bridge strain gauge. The RPM is measured by an AZDelivery infrared module (shown in green in Fig.2), triggered by reflective tape on the shaft, which provides a 5V TTL signal collected via a National Instruments cRio NI-9218 module at 50 kS/s/channel. An Arduino R2 was used to generate a PWM signal to control the ESC, communicating with the host PC via USB-serial communication.

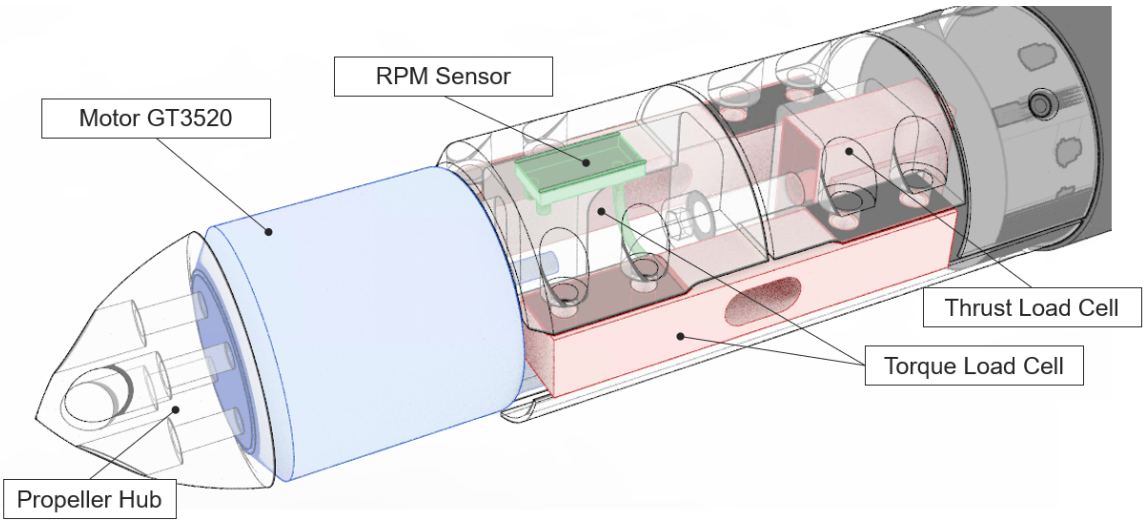

Figure 2 – Schematic outline of the propeller test bed utilized during the experiments. Load cells are shown in red, rpm sensor in green, motor in blue. The supportive structure is marked in black. The propeller hub and other aluminum parts are shown as transparent.

A Furness FCO-510 micromanometer measured the wind tunnel free stream velocity, as well as the ambient pressure and temperature. The ambient conditions in the tunnel were communicated to the host PC via LabVIEW Shared Variables and synchronized with the propeller data. Each data point is saved as the average of inputs during one second. Post-processing was done in MATLAB.

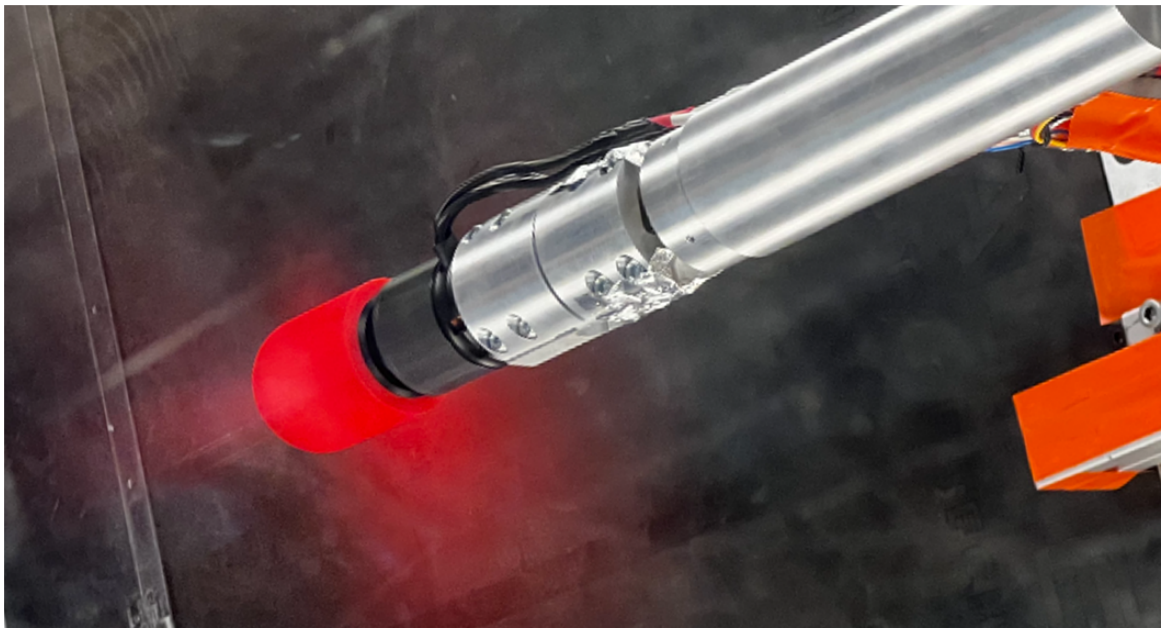

Figure 3 – Image of the V_3 propeller running in the wind tunnel during testing, seen through the transparent 20mm polycarbonate test chamber ceiling.

The torque load cells was calibrated by locking the rotation of the motor and mounting a calibrator where the propeller hub is mounted. A 100 g weight was gradually moved radially to create a negative, positive, and zero torque. The thrust sensor was calibrated axially. Before each measurement, the load cells were re-zeroed. The results of a torque sensor calibration are shown in Fig. 3 where a clear linear correlation can be found.

6. Results

The result section is divided into two main subsections. The numerical results (BEMT and CFD) are presented first, followed by wind tunnel results.

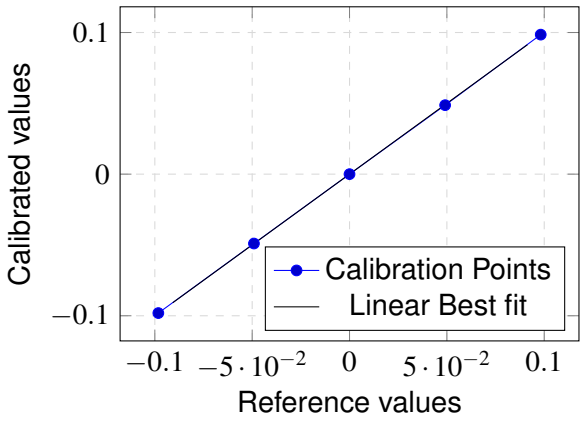

6.1 OPTOPROP

Figure 4(b) shows the propulsive efficiency η_p while varying the diameter for the current conditions and thrust requirements. The ideal propulsive efficiency using disc actuator theory is shown as blue dashed lines and marked as ideal in the legend. A similar investigation using a sweep of propeller diameters as design input to OTPOROP is shown using NACA-16 series and NACA four series and is shown Fig. 4(b).

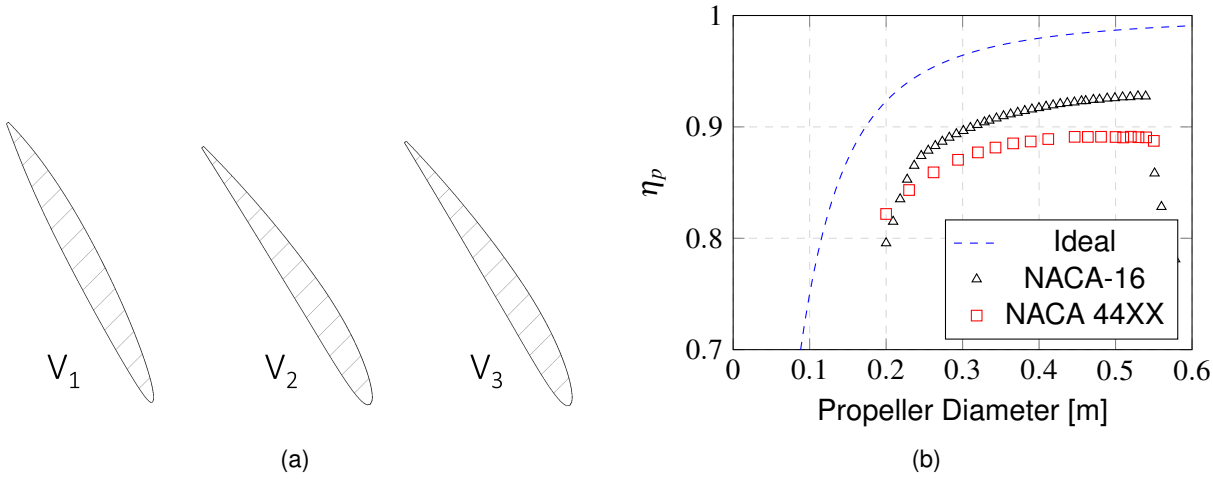

(a) (b)

Figure 4 – a) Airfoil cross-sections at 75% span. b) Comparison between the maximum propeller efficiencies computed for varying diameter and the corresponding ideal propeller efficiency. The dashed line represent results from disc theory, the colored points represent results from OPTOPROP.

A diameter of 0.389 m was selected during the design due to the diminishing returns in efficiency with the increase in diameter. The airfoil cross sections at 75% for the designs V_1, V_2 and V_3 designs are illustrated in Fig. 4(a). One may note the large difference between the NACA-16 (V_1) and the NACA-44 (V_2,V_3) airfoils. Propellers V_2 and V_3 are understandably similar as the only difference is a shift in the thrust requirement.

6.2 CFD and OPTOPROP Comparison

A comparison of results that denote key performance metrics predicted by CFD and OPTOPROP, at the design point, is presented for each specific propeller version (V_1, V_2 and V_3) in Table 5(b). Note the substantial difference between OPTOPROP and CFD for the V_1 propeller in both thrust and efficiency, compared to the V_2 and V_3 counterparts. The same results are shown in Fig. 5(a), provided as bar graphs to emphasize the difference between OPTOPROP and CFD for the three different designs.
It can be observed from Fig. 5, that the difference in efficiency between OPTOPROP and CFD are much smaller for the NACA 44-digit propeller compared to the NACA-16 propeller, where V_1 has a

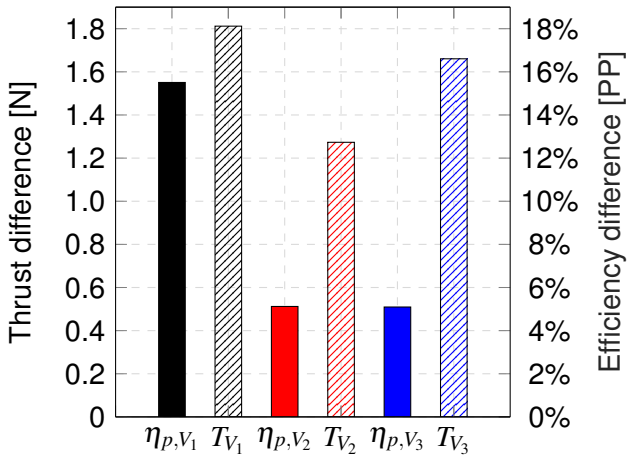

(a)

V_1 - NACA16	OPTOPROP	CFD
RPM [1/min]	3810	3810
J	1.012084	1.012084
η_p	91.53593%	76.02%
Thrust [N]	3.964	2.15216
V_2 - NACA4d	**OPTOPROP**	**CFD**
RPM [1/min]	3095	3095
J	1.245894	1.245894
η_p	88.690844%	83.5696%
Thrust [N]	3.964	2.6907
V_3 - NACA4d	**OPTOPROP**	**CFD**
RPM [1/min]	3400	3400
J	1.13413	1.13413
η_p	88.002764%	82.9068%
Thrust [N]	5.4	3.74

(b)

Figure 5 – Propeller efficiency vs. thrust using data from OPTOPROP and CFD simulations.

difference in efficiency of approximately 15%, whereas V_2 and V_3 only show a difference of approximately 5%.

6.3 Wind Tunnel Results

The thrust coefficient, power coefficient and efficiency data points retrieved from the wind tunnel tests are shown for V_1, V_2 and V_3 in Fig. 6-8 as a function of the advance ratio. The experimental data are compared with both OPTOPROP and CFD results at the operational design point. The estimated required C_T needed in order to meet the required thrust is marked with a dashed line in Fig. 6. Note that the flow effects are somewhat different in the wind tunnel compared to in the CFD solution. The experimental wind tunnel test data imply that the actual propeller performance is similar to the CFD data at the design point. In Fig. 8, the experimental efficiency data seem to flatten out at low advance ratios, as opposed to exhibiting a more typical parabolic curve shape. This behavior may have been caused by the significant elastic deformation of the blade observed at high blade loading.

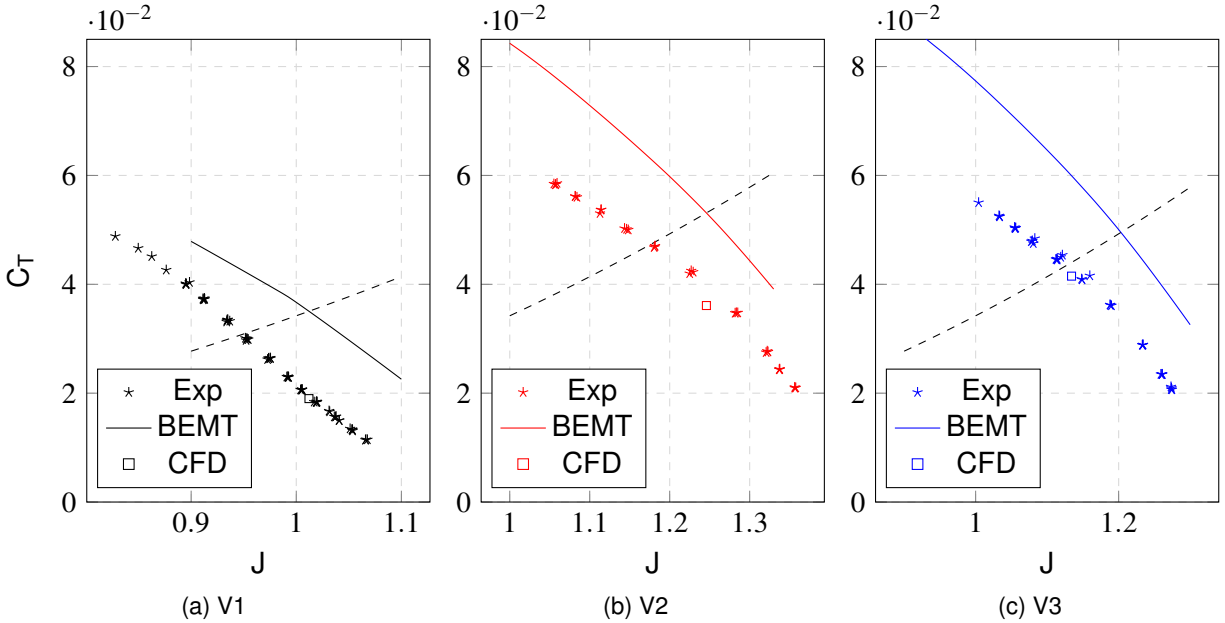

(a) V1 (b) V2 (c) V3

Figure 6 – Thrust coefficient vs. advance ratio. The dashed line marks the minimum required C_T.

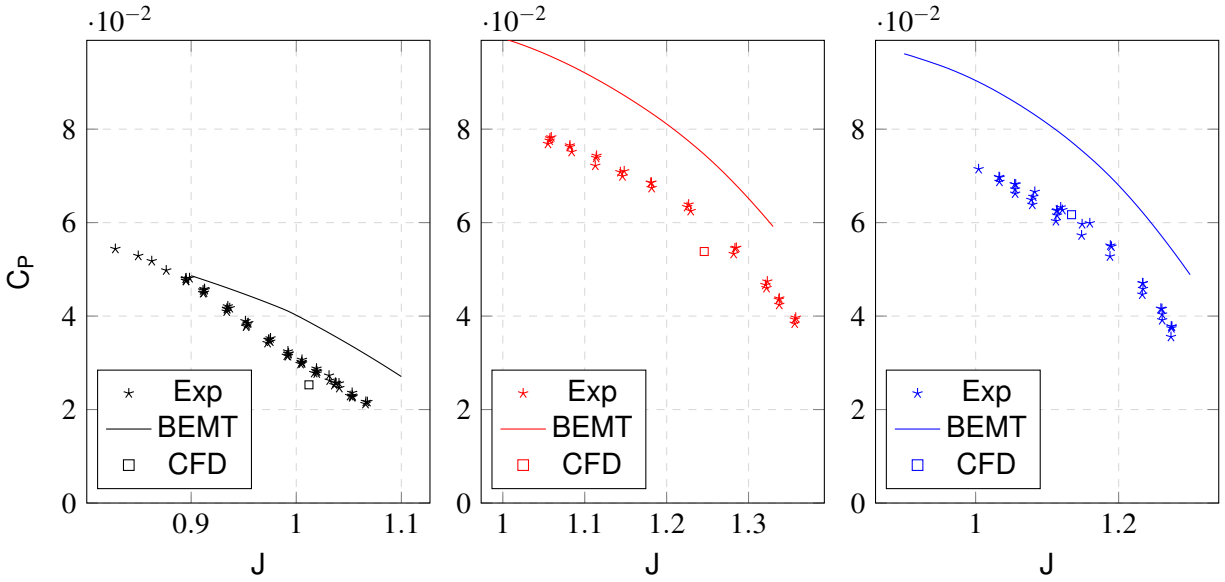

(a) V1 (b) V2 (c) V3

Figure 7 – Power coefficient vs. advance ratio.

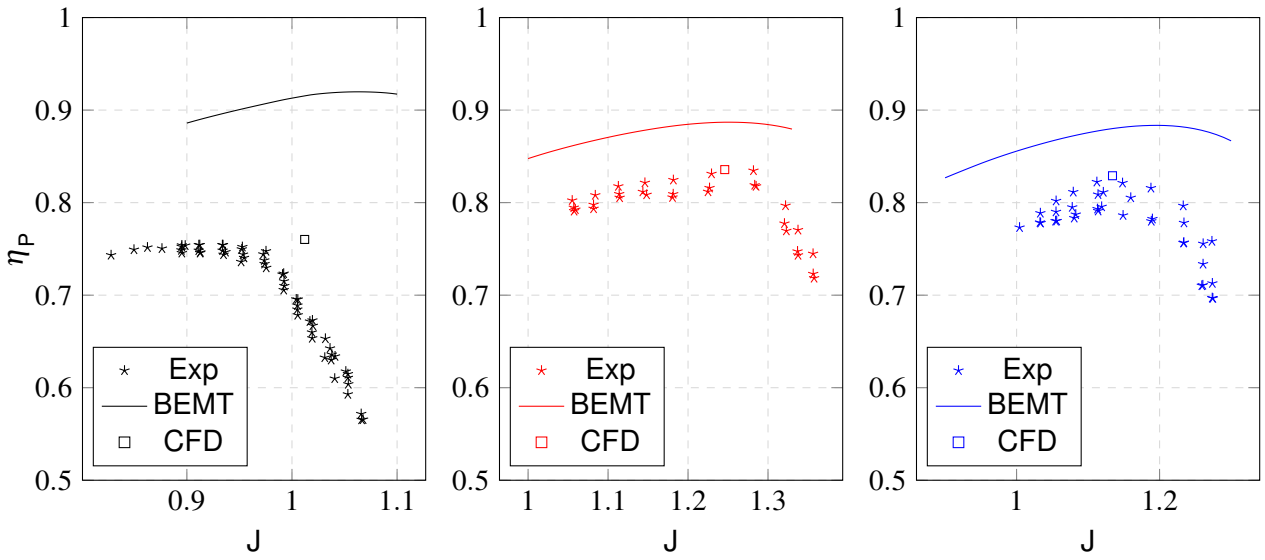

(a) V1 (b) V2 (c) V3

Figure 8 – Efficiency vs. advance ratio.

7. Conclusion

Three different propeller designs for a small UAV drone have been generated using the in-house design tool OPTOPROP, and was evaluated numerically and experimentally. The results emphasize the importance of accurate airfoil performance prediction data, with this study focusing on low-speed applications. Initial designs were generated using high-speed airfoil data, where substantial discrepancies between OTPOPROP and the numerical and experimental results were observed.

With accurate and representative airfoil data, OPTOPROP and CFD agrees within 5 percentage points in efficiency at design point.

The experimental results indicate the trends observed in the numerical simulations are correct. However, a direct comparison cannot be made as installation effects; such flow effects around the rig geometry and the 3D print surface roughness were not incorporated in the numerical simulation.

All designed propellers can provide sufficient thrust for the targeted mission. Both numerical and experimental data indicate that the final thrust-matched version, V_3, can achieve the desired thrust if operated at a slightly lower advance ratio relative to the design point. The efficiency of this propeller operating at the design point is superior compared to the best of-the-shelf propeller known to the authors.
Finally, since this work was done as part of a course, it has provided valuable hands-on experiences of applied research and contributed to enhancing the course content going forward.

8. Acknowledgement

We express our sincere gratitude to Alexandre Capitao Patrao for creating the OPTOPROP code used in this work. We also extend our thanks to the CASE association as well as Robert Sörensen for their invaluable assistance in manufacturing the 3D-printed propeller blades used in the experimental tests.

9. Copyright Statement

References

[1] C. N. Adkins and R. H. Liebeck. Design of optimum propellers. *Journal of Propulsion and Power*, 10(5):676–682, 1994.

[2] Airfoil Tools. Naca 4-digit airfoil generator. Accessed: November 20, 2023, `http://airfoiltools.com/airfoil/naca4digit`.

[3] T. Burdett, J. Gregg, and K. V. Treuren. An examination of the effect of reynolds number on airfoil performance. In *5th International Conference on Energy Sustainability & 9th Fuel Cell Science, Engineering and Technology Conference*, Washington, DC, USA, August 7-10 2011. Baylor University, Waco, TX, USA.

[4] B. N. D. M.F. Lindsey, D.B. Stevenson. Aerodynamic characteristics of 24 naca 16-series airfoils at mach numbers between 0.3 and 0.8. *NACA technical note No.1546*, 1948.

[5] P. Milten and C. Svensson. Design and evaluation of uav system to support naval search and rescue. Master's thesis, Chalmers University of Technology, 2022.

[6] A. C. Patrao. Implementation of blade element momentum/vortex methods for the design of aero engine propellers. Technical Report 2017:06, Chalmers University of Technology, 2017.

[7] V. T. Silva, A. Lundbladh, C. Xisto, P. Miltén, and I. Jonsson. Powered low-speed experimental aerodynamic investigation of an over-wing-mounted nacelle configuration. *Journal of Aircraft*, In Press, 2023.

[8] J. Stack. Tests of airfoils designed to delay the compressibility burble. *NACA technical note No.976*, 1939.